





# Estimation of the full shape of the crystalline lens from OCT: validation using stretched donor lenses

EDUARDO MARTÍNEZ-ENRÍQUEZ,<sup>1,\*</sup>  BIANCA MACEO HEILMAN,<sup>2,3</sup>  
ALBERTO DE CASTRO,<sup>1</sup>  ASHIK MOHAMED,<sup>4,5</sup>  MARCO  
RUGGERI,<sup>2</sup>  FERNANDO ZVIETCOVICH,<sup>6</sup>  FABRICE MANNS,<sup>2,3</sup>  
AND SUSANA MARCOS<sup>1,7</sup> 

<sup>1</sup>Instituto de Óptica, Consejo Superior de Investigaciones Científicas, Madrid, Madrid, Spain

<sup>2</sup>Ophthalmic Biophysics Center, Bascom Palmer Eye Institute, University of Miami School of Medicine, Miami, FL, USA

<sup>3</sup>Department of Biomedical Engineering, University of Miami College of Engineering, Coral Gables, FL, USA

<sup>4</sup>Ophthalmic Biophysics, LV Prasad Eye Institute, Hyderabad, Telangana, India

<sup>5</sup>Brien Holden Vision Institute, Sydney, NSW, Australia

<sup>6</sup>Department of Engineering, Pontificia Universidad Católica del Perú, Lima 15088, Peru

<sup>7</sup>Center for Visual Science. The Institute of Optics. Flaum Eye Institute, University of Rochester, Rochester, NY, USA

\*[eduardo.martinez@io.cfmac.csic.es](mailto:eduardo.martinez@io.cfmac.csic.es)

**Abstract:** Quantifying human crystalline lens geometry as a function of age and accommodation is important for improved cataract and presbyopia treatments. In previous works we presented *eigenlenses* as a basis of 3-D functions to represent the full shape of the crystalline lens *ex vivo*. Also, we presented the application of *eigenlenses* to estimate the full shape of the lens *in vivo* from 3-D optical coherence tomography (OCT) images, where only the central part of the lens -visible through the pupil- is available. The current work presents a validation of the use of *eigenlenses* to estimate *in vivo* the full shape of dis-accommodated lenses. We used 14 *ex vivo* crystalline lenses from donor eyes (11-54 y/o) mounted in a lens stretcher, and measured the geometry and the power of the lenses using a combined OCT and ray tracing aberrometry system. *Ex vivo*, the full extent of the lens is accessible from OCT because the incident light is not blocked by the iris. We measured in non-stretched (fully accommodated) and stretched (mimicking *in vivo* dis-accommodated lenses) conditions. Then, we simulated computationally *in vivo* conditions on the obtained *ex vivo* lenses geometry (assuming that just the portion of the lens within a given pupil is available), and estimated the full shape using *eigenlenses*. The mean absolute error (MAE) between estimated and measured lens' diameters and volumes were  $MAE = 0.26 \pm 0.18$  mm and  $MAE = 7.0 \pm 4.5$  mm<sup>3</sup>, respectively. Furthermore, we concluded that the estimation error between measured and estimated lenses did not depend on the accommodative state (change in power due to stretching), and thus *eigenlenses* are also useful for the full shape estimation of *in vivo* dis-accommodated lenses.

© 2023 Optica Publishing Group under the terms of the [Optica Open Access Publishing Agreement](#)

## 1. Introduction

The crystalline lens of the eye is able to change its shape dynamically to focus near and far objects in the retina (accommodation) [1]. The crystalline lens loses its accommodation ability and transparency with age, in what is known as presbyopia and cataract, respectively. The most common treatment for cataract involves removing the opacified crystalline lens and replacing it with an artificial intraocular lens (IOL) [2]. Emergent treatments for presbyopia, still under

development, include accommodative IOLs (A-IOLs) [3,4], which attempt to mimic the ability of the natural crystalline lens to change its shape (and thus its optical power) as a response of the action of the ciliary muscle, or pharmacological treatments to soften the crystalline lens material [5]. These solutions require that the ciliary muscle remains fairly functional with age [6]. Quantifying the human crystalline lens geometry, and its changes with accommodation and age, is key to improve current intraocular treatments for cataract and presbyopia, for example, obtaining more accurate predictions of the intraocular lens power [7,8] or size (in A-IOLs) to be implanted in a specific patient [3].

*Ex vivo*, some works have quantified the donor human crystalline lens geometry and its changes with age using different imaging techniques such as shadowphotography [9–12], corneal topography [13,14], magnetic resonance imaging (MRI) [15] and OCT [16–18]. In addition, the changes of the human crystalline lens shape can be studied with simulated dis-accommodation by stretching donors' eye lenses mounted in a lens stretcher system that simulates the action of the ciliary muscle pulling the lens capsule and zonulae equatorially [19].

*In vivo*, optical imaging techniques (such as Purkinje [20,21], Scheimpflug [22–25] and OCT [26–29]) have been used to quantify the shape of the crystalline lens within the pupil area, and have proved to be accurate once geometrical and optical distortions are corrected. A drawback of optical techniques is that the iris blocks the incident light preventing the imaging of the peripheral part of the lens. Non-optical techniques such as MRI [30–33] or Ultrasound Biomicroscopy (UBM) [34] allow visualization of the entire lens, but have some important drawbacks in comparison with optical techniques such as lower resolution, longer acquisition times, and typically require experienced operators. UBM requires contact of an ultrasound probe and the eye, typically through a gel. On the other hand, MRI is not available in an ophthalmology clinical setting.

The estimation of the full shape of the lens from the information visible through the pupil in optical techniques has been approached by extrapolating functions fitting the central part of the anterior and posterior surfaces of the lens and calculating the points of intersection. This so-called *intersection approach* is available in some commercial OCT systems such as the CASIA2 (Tomey, Nürenberg, Germany) and the Catalys laser (Johnson & Johnson Vision, Santa Ana, CA, USA), and has been recently used in some works to estimate the diameter or the equatorial plane position of the lens [35–38]. Nevertheless, we showed that the *intersection approach* overestimates the diameter and volume of the lens, and underestimates (anterior shift) the equatorial plane position [39].

In a previous work, we proposed a method for the 3-D crystalline lens full shape estimation from anterior segment OCT images *in vivo* (Martinez-Enriquez et al. [39]). The method relied on prior model training with a set of crystalline lenses *ex vivo*, and the lens shape was described by different functions for the anterior and posterior central zones, and the equatorial and peripheral regions. We have applied this method to quantify changes of crystalline lens full shape parameters (equatorial diameter, surface area, volume, etc.) *in vivo* as a function of accommodation [40], age [41], or myopia [42]. The method has also been applied to improve the estimation of the intraocular lens position in cataract surgery [7] and to quantify the crystalline lens full shape in a guinea pig model [43].

Recently, we have presented a different methodology (*eigenlenses*) that allows a compact representation of the full shape [44]. *Eigenlenses* consist of a basis of functions and weighting coefficients which can typically fit the full shape of the lens with great accuracy using less than 6 coefficients (with 6 coefficients, RMSE = 0.045 mm; explains the 96% of the variance in the training set). The *eigenlenses* functions are constructed from 3-D models of isolated human crystalline lenses *ex vivo* obtained using OCT images [18,44]. We have proposed a method based on the compaction ability of *eigenlenses* to estimate the full shape of the lens *in vivo* from OCT measurements in patients [45]. The *eigenlenses* method produced improvements

over our previous method [39] in terms of repeatability, robustness and computational cost. A possible criticism of this approach is that, while *eigenlenses* are constructed using a training set of isolated *ex vivo* lenses, and thus they are optimized to accurately represent *ex vivo* shapes, they are applied to describe the shape of the lenses in *in vivo* measurements. Isolated lenses are maximally accommodated, and, especially in younger eyes, their shape differs substantially from the stretched, dis-accommodated form. In previous work, we applied *eigenlenses* (trained on *ex vivo* isolated lenses) to estimate the full shape of the lens from *in vivo* OCT measurements [45]. However, a direct validation of the applicability of the *eigenlenses* representation in dis-accommodated lenses is missing.

In this study, we validate the use of *eigenlenses* to estimate the full shape of the lens *in vivo* under relaxed accommodation. *Ex vivo* lenses were mounted in a stretcher that simulates dis-accommodation. We used a combined custom-developed ray tracing aberrometry and 3-D OCT imaging system to obtain lens power and lens 3-D shape for the non-stretched (fully accommodated) and stretched (dis-accommodated) positions. The measured 3-D lens shape was compared to the shape retrieved from the *eigenlenses* method, assuming that only the central part of the lens was available (i.e., simulating *in vivo* conditions), allowing a direct validation of the method. We compared the accuracy in the estimation of the full shape using *eigenlenses* in the non-stretched and stretched conditions.

## 2. Methods

### 2.1. Combined OCT imaging, ray tracing aberrometry, and lens stretcher system

Several previous publications describe experimental implementations of an OCT imaging system, ray tracing aberrometry, and lens stretcher device [4,46]. In this work, we used a custom system set up at L V Prasad Eye Institute, previously reported in [46]. In brief, the system is comprised of a spectral domain OCT (SD-OCT) imaging subsystem that obtains the images that are analyzed for estimating the lens geometry, and a ray tracing aberrometry system (LRT) that senses wavefront aberrations of the lens with the OCT probing beam and is used to estimate the power of the lenses while simulating dis-accommodation with a motorized lens stretching system.

The SD-OCT (ENVISU R4400, Bioptigen Inc., NC) system is equipped with a superluminescent diode operating at a center wavelength of 880 nm. The axial range is 15.18 mm in air, with a pixel size of 7.4  $\mu\text{m}/\text{pixel}$ . The optical axial resolution of the system is 8.5  $\mu\text{m}$  in air. The lateral resolution of the system is 53  $\mu\text{m}$ . The effective acquisition speed is 32000 Ascan/s, and each 3-D volume was composed of 600 A-scans and 100 B-scans on a 15 mm x 15 mm lateral area.

The LRT system was programmed to perform a 6 mm x 6 mm raster scan centered on the lens by sequentially delivering 169 rays with 0.5 mm spacing [47]. The system uses a custom-built scanning telecentric beam delivery system that produces a focused beam with a 53  $\mu\text{m}$  spot diameter at the beam waist. The custom delivery probe is interfaced to the SD-OCT system. During the LRT experiment, a narrow beam was scanned across the lens and the slopes of the rays after passing through the lens at each incident position of the raster scan were acquired. Spot images were recorded along the optical axis for vertical heights ranging from 1 mm to 8 mm below the tissue chamber with an axial increment of 1 mm. An imaging sensor (DCC1545M-GL, Thorlabs, Newton, New Jersey) mounted below the tissue chamber on a two-dimensional (X-Z) motorized positioning records the spots, corresponding to the cross-section of the laser beam, at the various heights below the tissue chamber. The position of the centroids of the spots was used to calculate the slope of each ray exiting the lens, thereby allowing the calculation of lens power. The LRT data acquisition was fully automated using a custom LabView program (National Instruments Corporation, Austin, TX, USA).

A custom-built tissue chamber was developed to hold a motorized lens stretching system for simulating accommodation. A detailed description of the lens stretching system can be found in a previous publication [46]. To briefly summarize, the system consists of a manual lens stretcher

(STR-MS-B, Bioniko Consulting LLC, FL) combined with a geared micro servo motor enabling the motorized stretching of the ocular tissue. The lens stretcher applies a radial stretching force to the sclera to simulate dis-accommodation and can be programmed to displace the sclera radially in a step-wise fashion.

## 2.2. *Ex vivo* human lenses and experimental protocol

Fourteen human donor globes (11-54 y/o, mean =  $34 \pm 11$  y/o) from the Ramayamma International Eye Bank at LV Prasad Eye Institute (Hyderabad, India) were dissected to preserve the lens with its accommodating framework and sclera. The tissue was mounted in the motorized miniature lens stretcher system and immersed in a cuvette filled with balanced salt solution (BSS, Alcon Laboratories, Inc., Fort Worth, TX, USA). The system simulated dis-accommodation by radial stretching of the outer sclera. 3-D OCT images and LRT measurements were acquired at 0 and 2 mm of stretching, quantified as the change in outer scleral diameter. Tissue handling was performed following published protocols to minimize water uptake (and thus swelling) [18].

## 2.3. 3-D models construction of *ex vivo* lenses

Figure 1 shows the main steps for the construction of crystalline lens 3-D models *ex vivo* from OCT raw images, namely: automatic segmentation of the images; registration of the different B-scans to obtain the 3-D model (in pixels); conversion to millimeters, including fan and optical distortion correction; tilt removal and extrapolation (when needed).

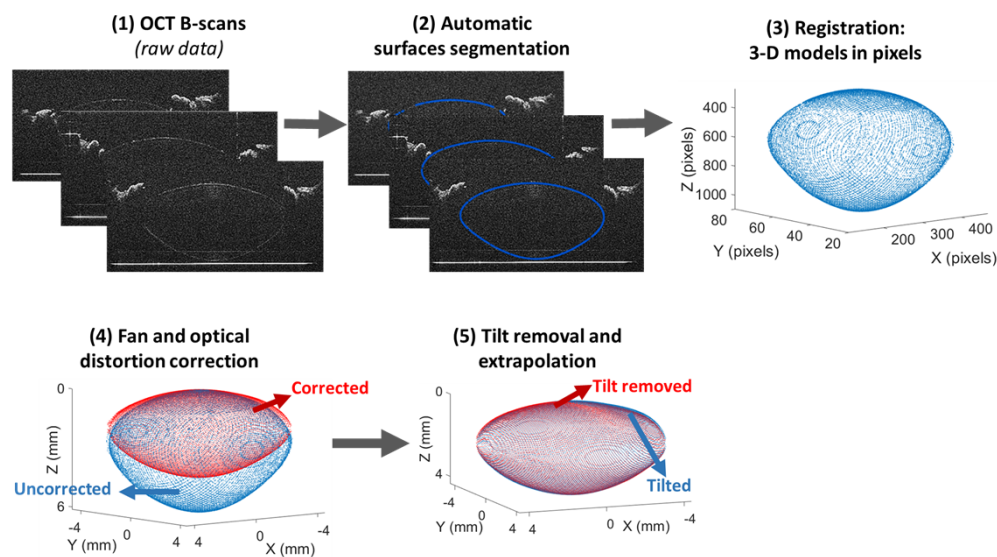


**Fig. 1.** *Ex vivo* 3-D models construction, including: (1) OCT B-scans; (2) Automatic surfaces segmentation; (3) Registration of the B-scans to obtain the 3-D models in pixels; (4) Fan and optical distortion correction; (4) Tilt removal and extrapolation of the most peripheral part (when needed).

In the segmentation process, the contour of the full lens was automatically detected with an algorithm extended from previous works [18,40]. In short, edges are first detected and a 4-th order Zernike fitting is applied to the resulting 3-D data to smooth the surfaces. The resulting smooth surface is then used to guide a new refined segmentation in each B-scan. In this work, this process was repeated for three different orientations of the crystalline lenses, obtaining the full 3-D shape of the lens. Each 3-D full lens was converted to millimeters (using the calculated

lateral and axial pixel sizes) and corrected for fan distortion [46,48] and optical distortion (due to imaging the anterior surface of the lens through the preservation media and the posterior surface through the lens). We used  $n = 1.341$  as the group refractive index of the BSS (at 880 nm) [46], and the average refractive index for each crystalline lens, calculated using the method in [16]. Finally, the tilt was removed by rotating the lens by the angle that the lens equatorial plane subtends with respect to the XY-reference axis, and the most peripheral region of the lens was then generated using extrapolation in the cases when these regions were not captured in the OCT image.

#### 2.4. Full shape estimation from the central part using *eigenlenses*

Figure 2 shows the procedure to evaluate the accuracy of the estimation of the lenses full shape from their central part using *eigenlenses*. We performed the following steps:

- 1) Simulation of *in vivo* conditions in the crystalline lens 3-D models obtained from *ex vivo* lenses, assuming that only the central part (for a given pupil diameter) is visible.
- 2) Application of the *eigenlenses* method to estimate the full shape of the lens from central part data, as described in detail in [45].
- 3) Comparison of the quantified geometrical parameters from the estimated full shape using *eigenlenses* with the same parameters from the actual geometry experimentally measured (the *ex vivo* 3-D models).

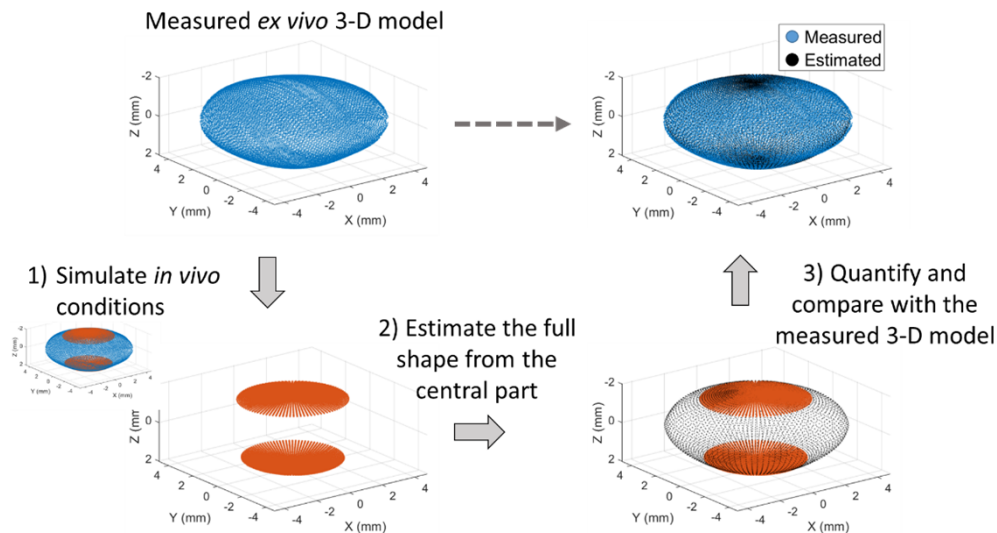


**Fig. 2.** Procedure to evaluate the accuracy of the *eigenlenses* method in the estimation of the lenses full shape from their central part. In the example, we assumed a pupil of 5 mm of diameter.

This process was applied for each individual lens in the non-stretched and stretched conditions.

#### 2.5. Full shape geometry quantification

Once the full shape 3-D models were constructed or estimated, various biometric parameters of the lens were quantified. Specifically, we obtained: (1) lens thickness (LT); (2) radius of curvature of anterior lens surface (RAL); (3) lens equatorial diameter (DIA); (4) lens volume (VOL); and (5) shape factor, defined as the ratio LT/DIA. The RAL was obtained fitting a sphere



calculated in a 6-mm diameter optical zone; the VOL was estimated by numerically solving the double integration of the anterior and posterior lens surfaces [40].

## 2.6. Power estimation from LRT measurements

The LRT images were processed using a custom MATLAB program (Mathworks, Natick, MA, USA) to find the centroid of each spot. The centroid positions were used to estimate the X-Y coordinates of the ray incident on the imaging sensor. The coordinates of the spots acquired at the 8 axial positions were used to determine the ray slope in the X and Y directions for each individual ray by performing a linear regression of the X and Y coordinates of the spots. The rays exiting the lens were reconstructed using these ray slopes, the incident ray position, and the correction for refraction through the window separating the BSS and air. The ray with zero slope was selected as the center ray for the RMS spot size calculation. The central 3-mm zone of the lens (49 rays) was used to solve for the position where the RMS spot size for the reconstructed rays was minimized. This position was used as an estimate of the best focus,  $z_{\text{focus}}$ . The power of the lens was calculated as:

$$\text{Power (D)} = 1.341/z_{\text{focus}}$$

where 1.341 is the group refractive index of BSS. The lens power was calculated for the lenses at non-stretched and stretched positions.

## 2.7. Data analysis

We analyzed the relationship between the stretching-induced geometrical changes and power changes using linear regression analysis (Pearson correlation coefficient,  $\rho$ ; and the p-value for testing the hypothesis of no correlation,  $p$ ). We also used linear regression to analyze the relationship between power changes and age.

We studied the agreement between the geometrical parameters estimated using the *eigenlenses* method and those measured directly from the full shape *ex vivo* models, by means of Bland-Altman plots [49]. We investigated if the estimation error was significantly different in non-stretched and in stretched lenses, and when using different full shape estimation methods, by means of a t-test. We also investigated the relationship between estimation error and accommodation amplitude using linear regression. For all analyses, statistical significance was defined as a p-value lower than 0.05. Calculations were obtained using MATLAB software.

# 3. Results

## 3.1. OCT images and 3-D full shape models

Figure 3 shows an example of a central B-scan acquisition and the 3-D full shape model in a 28-year old lens mounted in a stretcher, for the non-stretched (fully accommodated, Fig. 3(a) upper panel) and stretched (dis-accommodated, Fig. 3(a), lower panel) conditions. The crystalline lens reconstructed 3-D models for the non-stretched (black) and stretched (blue) conditions are presented superimposed for comparison purposes (Fig. 3(b)).

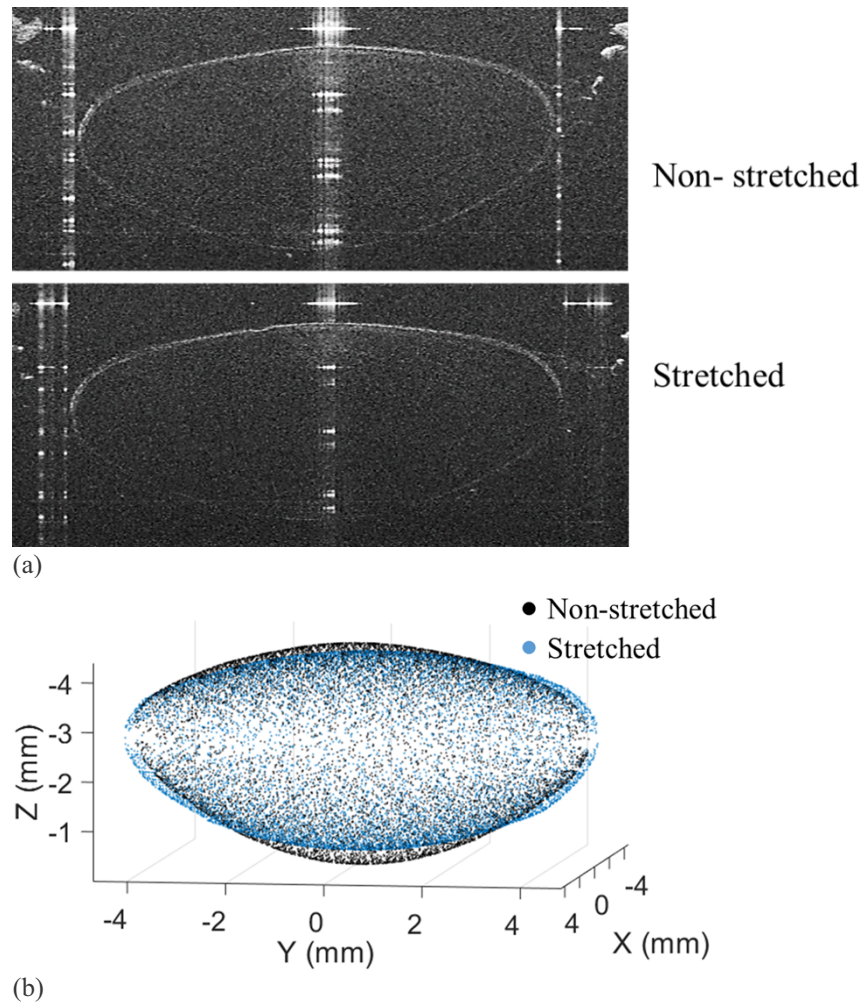
## 3.2. Relationship between geometry changes and power changes

Figure 4 shows the correlation between geometrical parameters changes ( $\Delta\text{Parameter}$ ) and power changes ( $\Delta\text{Power}$ ) produced by the stretching. Changes are defined as:

$$\Delta\text{Parameter} = \text{Parameter}_{\text{stretched}} - \text{Parameter}_{\text{non-stretched}}$$

$$\Delta\text{Power (D)} = \text{Power}_{\text{stretched}} - \text{Power}_{\text{non-stretched}}$$

Note that this is equivalent to calculating the difference between the parameter at the dis-accommodated position (stretched) and the parameter at a fully accommodated position



**Fig. 3.** (a) Example of cross-sectional OCT images of a 28-year old donor lens mounted in the stretcher. Top: non-stretched position; Bottom: stretched position. (b) 3-D models of the non-stretched (black) and stretched (blue) states for the same lens.

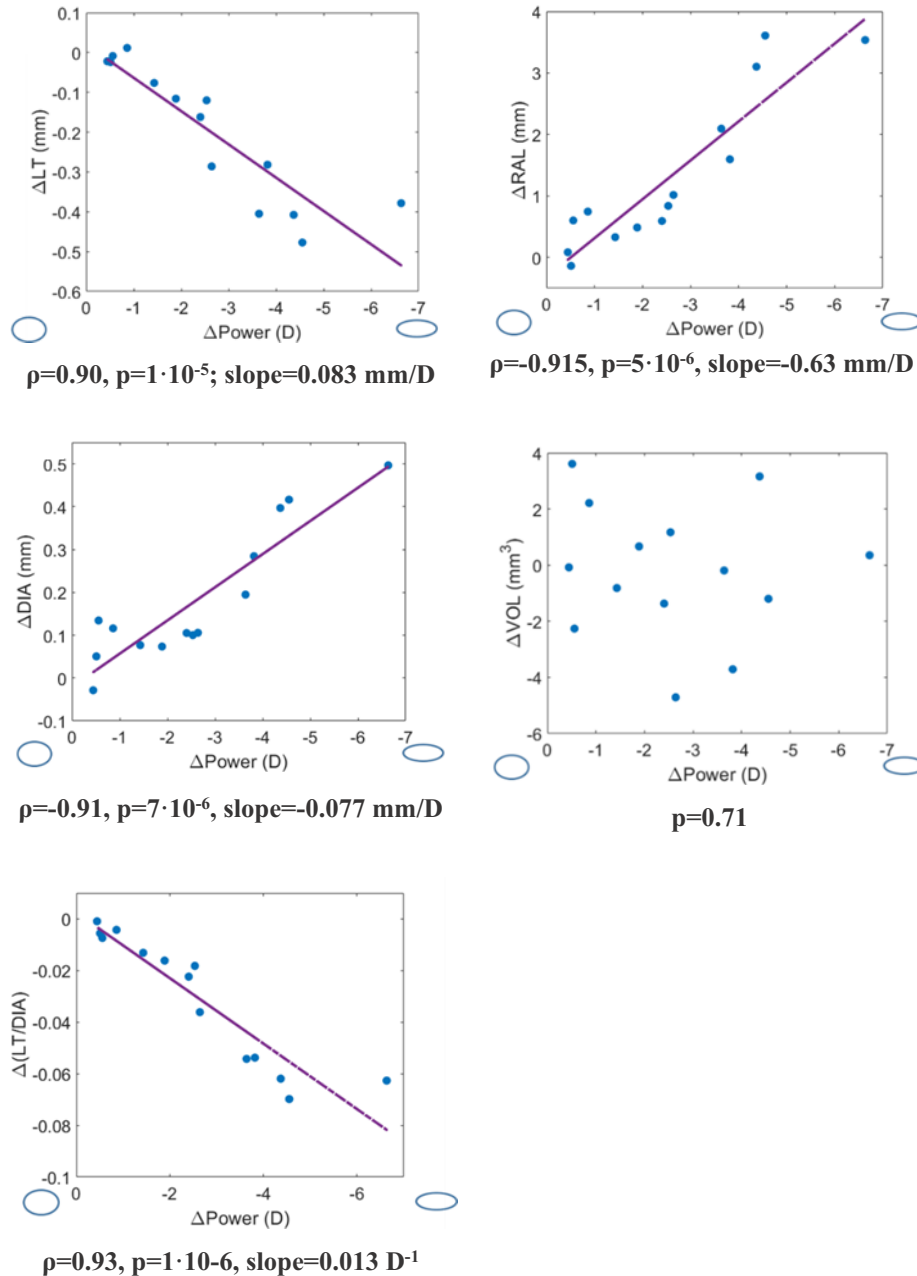


**Fig. 4.** Correlation between geometrical changes and change in power for the 14 lenses included in the study. The purple solid line represents the best linear fitting when the correlation is statistically significant. Correlation coefficient ( $\rho$ ), the p-value for testing the hypothesis of no correlation ( $p$ ) and the slope are also shown. Ellipses in blue in the X axis depict the accommodative state (rounder are accommodated or unstretched lenses, flatter are dis-accommodated or stretched lenses). LT: Lens thickness; RAL: Radius of curvature of anterior lens surface; DIA: Lens equatorial diameter; VOL: Lens volume.



(non-stretched). The analyzed parameters are LT, RAL, DIA, VOL, and DIA/LT ratio, each represented in a different panel. The purple solid lines in some panels represent the best linear fitting when the correlation is statistically significant. The values below each graph represent the correlation coefficient ( $\rho$ ), the p-value for testing the hypothesis of no correlation (p), and the slope. Note that more negative values are shown from left to right in the X axis for convenience.

### 3.3. Comparison between measured and estimated full lens shape

Calculated lens parameters from the direct measurements of the entire lens and estimates from the central pupillary region (assuming pupil diameters of 4.4 mm, 5.2 mm and 5.9 mm) were compared using Bland-Altman (Fig. 5; DIA, left panels; VOL, right panels). A total of 28 lenses were compared, including 14 stretched (red diamonds) and 14 non-stretched (blue points) conditions. The Y axis in each figure represents the difference between the estimated DIA or VOL using the *eigenlenses* and the measured value of the same parameter. The limits of agreement (LoA) are calculated as  $1.96 \cdot SD$ , where SD is the standard deviation of the differences. Upper, middle, and lower panels represent results for different widths of the central zone, corresponding to pupil diameters of 4.4 mm, 5.2 mm and 5.9 mm.

Table 1 shows the mean estimation error (ME)  $\pm$  standard deviation and the mean estimation absolute error (MAE)  $\pm$  standard deviation for DIA and VOL and different pupil diameters. Table 2 shows the correlation for DIA and VOL between the estimated and measured lenses.

**Table 1. Mean estimation error (ME)  $\pm$  standard deviation and mean estimation absolute error (MAE)  $\pm$  standard deviation for DIA (mm) and VOL (mm<sup>3</sup>) using 3 different pupil diameters. The estimation error is calculated as the difference between the estimated parameter using the *eigenlenses* and the measured value.**

Pupil diameter (mm)	DIA (mm)	VOL (mm <sup>3</sup> )
4.4 mm	ME = $0.08 \pm 0.34$	ME = $1.1 \pm 9.6$
	MAE = $0.29 \pm 0.20$	MAE = $7.8 \pm 5.5$
5.2 mm	ME = $0.09 \pm 0.31$	ME = $1.2 \pm 8.4$
	MAE = $0.26 \pm 0.18$	MAE = $7.0 \pm 4.5$
5.9 mm	ME = $0.08 \pm 0.29$	ME = $1 \pm 7.4$
	MAE = $0.24 \pm 0.17$	MAE = $6.3 \pm 3.9$

**Table 2. Correlation between the DIA and VOL of estimated and measured lenses. Correlation coefficient ( $\rho$ ) and the p-value for testing the hypothesis of no correlation (p) are indicated.**

Pupil diameter (mm)	DIA (mm)	VOL (mm <sup>3</sup> )
4.4 mm	$\rho = 0.71, p < 0.05$	$\rho = 0.92, p < 0.05$
5.2 mm	$\rho = 0.76, p < 0.05$	$\rho = 0.94, p < 0.05$
5.9 mm	$\rho = 0.79, p < 0.05$	$\rho = 0.95, p < 0.05$

### 3.4. Dependency of the estimation error with accommodative power

To validate the ability of the *eigenlenses* method to estimate the full shape of lenses in different accommodative states, we analyzed the relationship between the estimation error and the accommodative state (change in power due to stretching). We did not find a correlation between the estimation error and  $\Delta Power$  for DIA or VOL for any of the tested pupil diameters (linear regression,  $p > 0.05$ ). Furthermore, we did not find a statistically significant difference between the mean estimation error for the stretched and non-stretched lenses (t-test,  $p > 0.05$ ).

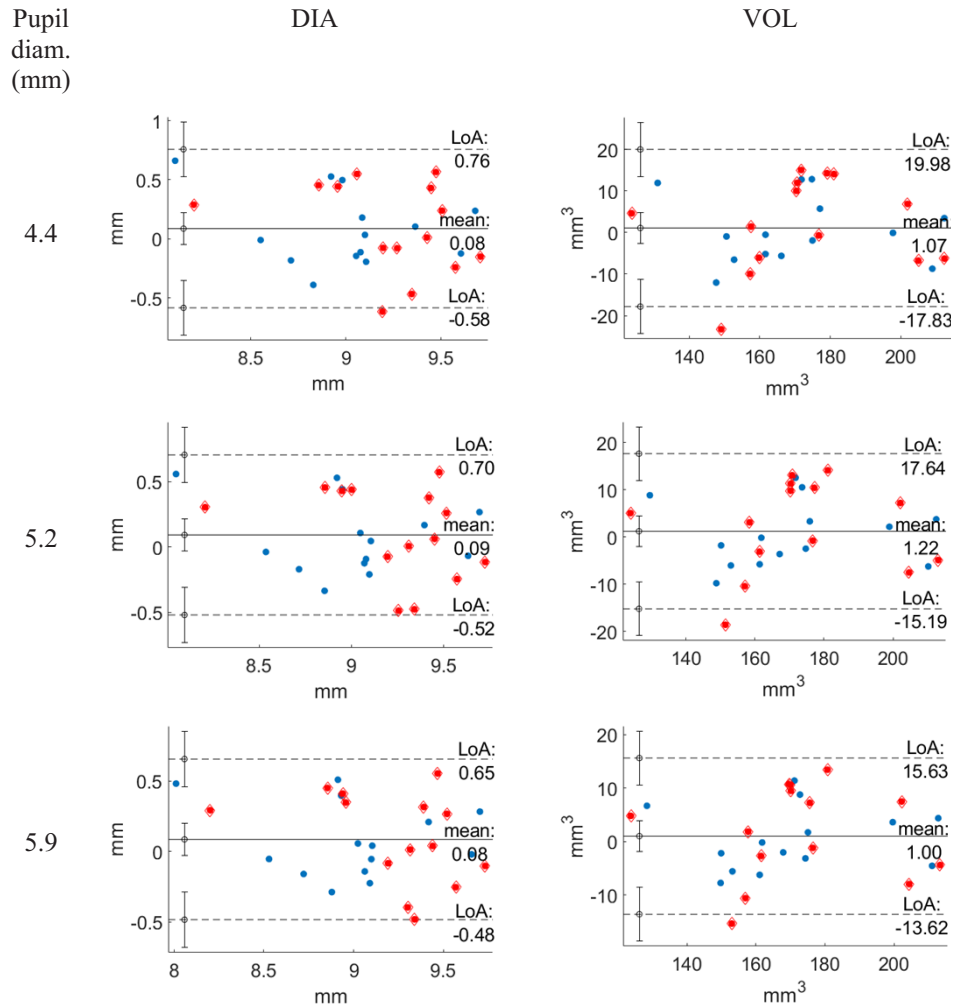


**Fig. 5.** Bland-Altman plots for the DIA (first column) and VOL (second column) calculated from lens full shape estimated with *eigenlenses* and measured. Red diamonds represent stretched lenses and blue points non-stretched lenses. Y axis: difference between the estimation using the *eigenlenses* and the measured value; LoA: Limit of Agreement ( $1.96 \cdot \text{SD}$ , where SD is the standard deviation of the differences).

### 3.5. Relationship between *eigenlenses* coefficients changes and power changes

We studied the correlation between *eigenlenses* coefficients changes ( $\Delta a_k = a_{k, \text{stretched}} - a_{k, \text{non-stretched}}$ ) and power changes ( $\Delta \text{Power}$ ) produced by the stretching. From the analyzed coefficients ( $\Delta a_1$  to  $\Delta a_6$ ), only  $\Delta a_1$  and  $\Delta a_2$ , represented in Fig. 6, showed statistically significant correlations. Results shown correspond to a 5.9 mm pupil.

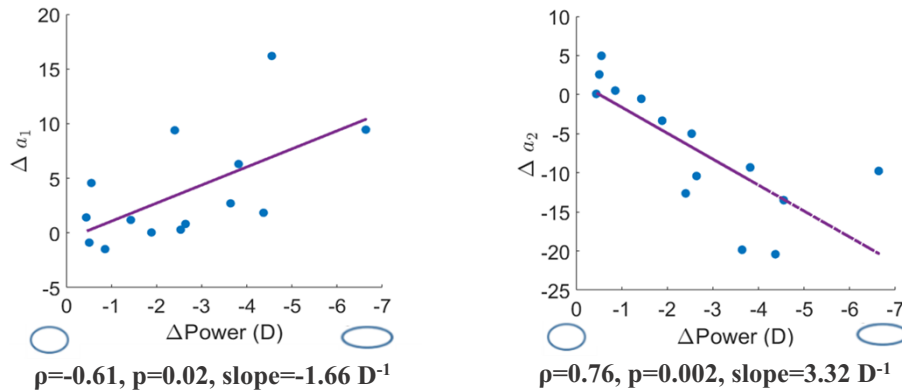


**Fig. 6.** Correlation between *eigenlenses* coefficients changes and change in power for the 14 lenses included in the study. Left:  $\Delta a_1$ ; Right:  $\Delta a_2$ . The purple solid line represents the best linear fitting. Correlation coefficient ( $\rho$ ), the p-value for testing the hypothesis of no correlation ( $p$ ) and the slope are also shown. Ellipses in blue in the X axis depict accommodative state (rounder are accommodated or unstretched lenses, flatter are dis-accommodated or stretched lenses).

Left part of the figure shows  $\Delta a_1$ , and right part  $\Delta a_2$ . The purple solid lines represent the best linear fitting. The values below each graph represent the correlation coefficient ( $\rho$ ), the p-value for testing the hypothesis of no correlation ( $p$ ), and the slope. Note that more negative values are shown from left to right in the X axis for convenience.

We also obtained an expression for the estimation of  $\Delta \text{Power}$  as a function  $\Delta a_1$  and  $\Delta a_2$  using multivariate linear regression:

$$\Delta \text{Power} = -1.14 - 0.13 \times \Delta a_1 + 0.14 \times \Delta a_2.$$

Using this linear model, we obtained a coefficient of determination  $R^2 = 0.68$ .

## 4. Discussion

Recently we presented the novel concept of *eigenlenses* [44] and demonstrated its application for the *in vivo* estimation of the full shape of the crystalline lens from its central part, available in OCT images [45]. As *eigenlenses* are constructed using a training set of isolated *ex vivo* lenses (fully accommodated), an open question remained about their ability to represent *in vivo* measurements in a dis-accommodated form (relaxed). In this paper, we validated the accuracy of *eigenlenses* for estimating the full shape of lenses in a relaxed accommodation state using donor lenses mounted in a lens stretcher.

The MAE between the DIA and VOL measured and estimated with *eigenlenses* decreased when the pupil diameter increased, which was expected, as with larger pupil diameters more information is available for the estimation. The DIA estimation error decreased from around  $\text{MAE} = 0.29 \pm 0.20 \text{ mm}$  (4.4 mm pupil) to  $0.24 \pm 0.17 \text{ mm}$  (5.9 mm pupil) and the VOL estimation error decreased from  $\text{MAE} = 7.8 \pm 5.5 \text{ mm}^3$  to  $6.3 \pm 3.9 \text{ mm}^3$ . Note that when we performed the same analysis in 103 *ex vivo* isolated lenses (in a fully accommodated state) used for the

*eigenlenses* construction [44], we obtained slightly lower mean estimation errors ranging from  $MAE = 0.22 \pm 0.15$  (4.4 mm pupil) to  $0.19 \pm 0.13$  mm (5.9 mm pupil) in DIA and  $MAE = 5.8 \pm 4$  mm<sup>3</sup> (4.4 mm pupil) to  $4.6 \pm 3$  mm<sup>3</sup> (5.9 mm pupil) in VOL. This is probably due to the fact that (i) these lenses were the ones used for the construction of the *eigenlenses*, and thus we are evaluating the error in the same set of lenses used to train the models; and (ii) slight tilt or asymmetric stretching of the lens in the lens stretcher which is not a factor when imaging isolated lenses.

We did not find a statistically significant correlation between the DIA and VOL mean estimation errors and the measured  $\Delta Power$  (linear regression,  $p > 0.05$ ), nor differences in the mean error between fully stretched and non-stretched lenses (t-test,  $p > 0.05$ ), indicating that the estimation error does not depend on the accommodative state and that the model can be used to predict the full shape in *in vivo* lenses under relaxed accommodation. This is one of the most important conclusions of the study.

The MAE for VOL and DIA obtained with the *eigenlenses* method was significantly lower (t-test,  $p < 0.05$ ) than the one obtained using the *intersection approach* in the same set of lenses for all the tested pupils. For example, for the 5.9 mm pupil, the error with the *intersection approach* was  $MAE = 1.44 \pm 0.56$  mm for DIA and  $MAE = 20 \pm 14$  mm<sup>3</sup> for VOL. When we compared the MAE obtained with *eigenlenses* and with our previous method for full shape estimation [39], *eigenlenses* outperformed the previous method for all the tested pupils (for example, the error with [39] was  $MAE = 0.35 \pm 0.29$  mm for DIA and  $MAE = 9 \pm 8$  mm<sup>3</sup> for VOL for the 5.9 mm pupil). Thus, our method could be implemented in clinically available OCT systems to improve full shape geometrical parameters estimation. This can be useful for improving the estimation of the IOL position in a cataract surgery [7] as well as the size to be implanted in accommodative IOLs for presbyopia.

We obtained statistically significant correlations between changes in the coefficients ( $\Delta a_1$  and  $\Delta a_2$ ) and the  $\Delta Power$  produced by the stretching, with the stronger correlation for the  $\Delta a_2$  coefficient ( $\rho = 0.76$ ,  $p = 0.002$ ). We found that  $a_1$  increased and  $a_2$  decreased with stretching (lower power). These findings agree with the results obtained in our previous works [44,45]. When we estimated  $\Delta Power$  as a function  $\Delta a_1$  and  $\Delta a_2$  using multivariate linear regression, the estimation model improved in comparison with using just a single coefficient. Nevertheless, additional factors might contribute to optical power (i.e., variations of the gradient index of refraction, GRIN, with age) that are not accounted for in the model.

We analyzed the geometrical changes of the *ex vivo* crystalline lens in the stretcher as a function of the changes of the measured power (Fig. 4) and found that they were similar to the ones expected in physiological accommodation. Specifically, we found that the anterior lens radius decreased  $-0.63$  mm/D, similarly to the mean change per diopter of  $-0.61$  mm/D reported by Dubbelman et al. [25] with accommodation. The lens thickness increased  $0.08$  mm/D, which matches with values reported *in vivo* using MRI (Khan et al.,  $0.08$  mm/D [50]; Sheppard et al.,  $0.08$  mm/D [33]) and OCT (Martinez-Enriquez et al.,  $0.07$  mm/D [40]). The lens diameter decreased  $-0.077$  mm/D, that matches with works with MRI (Khan et al.,  $-0.07$  mm/D; Sheppard et al.,  $-0.09$  mm/D; Jones et al.,  $-0.07$  mm/D [51]) and OCT full shape estimation methods ( $-0.13$  mm/D using accommodative response [40];  $-0.07$  mm/D in an emmetropic group [45]). Finally, changes in lens volume with stretching were not statistically significant, as expected and found in previous *in vivo* literature using OCT [45] and MRI [31].

When we analyzed geometrical changes of the *ex vivo* stretched lenses of this study as a function of age, we found that the deformations were larger in younger lenses than in older lenses and that the lens volume remained constant with stretching at all ages [52]. We found a high correlation between power changes and age for ages between 28 and 45 y/o ( $\rho = 0.82$ ,  $p = 0.01$ ; slope =  $0.26$  D/year). The obtained slope was similar to the one reported by Kasthurirangan et al. [53] for physiological accommodation. Finally, the correlation between geometrical parameters

and age for the non-stretched state was similar to the one reported in isolated lenses in [18] (linear correlation is calculated in the linear range of changes, from approximately 20 y/o).

The current study had the following limitations. Some lenses were discarded because the posterior lens or the periphery of the lens were not visible in the OCT images. The changes in some lenses with stretching were small due to experimental difficulties (this occurred also in young lenses). Even in cases where the lens was correctly stretched, we could not guarantee that full dis-accommodation was achieved, i.e., that the stretching produced 0 D accommodative state (far vision). However, this fact did not affect the analysis of geometrical changes of the crystalline lens as a function of the changes of the measured power (obtained from the LRT): if a small deformation was induced by the stretcher, the power change measured was also small. In the analysis of correlations with age presented above, we took only the points in the “convex hull” (i.e., for a given age, we took the points with maximum deformation). Finally, the GRIN was not considered when reconstructing the shape of the posterior surface of the lens. This issue was solved in previous works by measuring the anterior surface of the lens facing the OCT beam (anterior-up measurements), flipping the lens, measuring the posterior surface facing the OCT beam (posterior-up measurements), and then registering both measurements [18,44]. In this work we did not have posterior-up measurements for all the lenses and stretched states. This is the reason why we didn’t present here results for the radius of curvature of the posterior lens. The measurement of the radius of curvature of the anterior lens and lens diameter were not affected by this approximation. Furthermore, in [39] we proved that the influence of this approximation in the estimated volume was negligible. Finally, note that the results presented in this study reproduced the same conditions that are accessible in *in vivo* measurements, where the GRIN is usually ignored to reconstruct the posterior surface of the lens.

## 5. Conclusion

We have validated our method for the estimation of the full shape of the crystalline lens from OCT images for *in vivo* relaxed accommodation lenses. First, we measured *ex vivo* lenses mounted in a lens stretcher and demonstrated that this condition simulated *in vivo* relaxed accommodation. Then, we simulated *in vivo* conditions on these measurements (assuming that only the central part of the lens visible through the pupil was available) and compared our estimation of the full shape with the measured lens shape. Using these results, we demonstrated that the estimation error did not depend on the accommodative state, and thus, the method can be applied *in vivo* with the same accuracy as *ex vivo* lenses. Finally, we have shown that the method outperformed state of the art full shape estimation methods implemented in commercial OCTs.

This framework can be applied to generate accurate patient-specific models of the crystalline lens *in vivo*, which has the potential to improve cataract surgery (more accurate selection of IOL power) and the design of solutions to restore accommodation (accommodative IOLs).

**Funding.** European Project IMCUSTOMEYE H2020-ICT-2017 Ref. 779960; European Project SILKEYE H2020-ERC-2018-ADG Ref. 833106; Spanish government grant PID2020-115191RB-I00; NIH grants P30; Research to Prevent Blindness Departmental Funds to Flaum Eye Institute and Bascom Palmer Eye Institute; NIE P30EY 001319; Unrestricted Funds to Research to Prevent Blindness, NY; National Institutes of Health Center Core Grant (R01EY021834); Florida Lions Eye Bank and Beauty of Sight Foundation; Hyderabad Eye Research Foundation.

**Disclosures.** EME (P), SM (P).

**Data availability.** Data underlying the results presented in this paper are available in the “Estimation of the full shape of the crystalline lens from OCT: validation using stretched donor lenses” repository [54].

## References

1. D. A. Atchison and G. Smith, *Optics of the Human Eye*, (Butterworth-Heinemann, 2000).
2. S. Marcos, E. Martinez-Enriquez, M. Vinas, A. de Castro, C. Dorronsoro, S. P. Bang, G. Yoon, and P. Artal, “Simulating outcomes of cataract surgery: important advances in ophthalmology,” *Annu Rev Biomed Eng* **23**(1), 277–306 (2021).



3. J. L. Alió, J. L. Alió del Barrio, and A. Vega-Estrada, "Accommodative intraocular lenses: where are we and where we are going," *Eye and Vision* **4**(1), 16 (2017).
4. A. de la Hoz, J. Germann, E. Martinez-Enriquez, D. Pascual, N. Bekesi, N. Alejandre-Alba, C. Dorronsoro, and S. Marcos, "Design and ex situ performance of a shape-changing accommodating intraocular lens," *Optica* **6**(8), 1050–1057 (2019).
5. N. Haghpanah and R. Alany, "Pharmacological treatment of presbyopia: a systematic review," *Eur J Transl Myol* **32**(3), 10781 (2022).
6. J. Tabernero, E. Chirre, L. Hervella, P. Prieto, and P. Artal, "The accommodative ciliary muscle function is preserved in older humans," *Sci. Rep.* **6**(1), 25551 (2016).
7. E. Martinez-Enriquez, P. Perez-Merino, S. Duran-Poveda, I. Jimenez-Alfaro, and S. Marcos, "Estimation of intraocular lens position from full crystalline lens geometry: towards a new generation of intraocular lens power calculation formulas," *Sci. Rep.* **8**(1), 9829 (2018).
8. T. Olsen and P. Hoffmann, "C constant: new concept for ray tracing-assisted intraocular lens power calculation," *J. Cataract Refract. Surg.* **40**(5), 764–773 (2014).
9. R. Urs, F. Manns, A. Ho, D. Borja, A. Amelinckx, J. Smith, R. Jain, R. Augusteyn, and J. M. Parel, "Shape of the isolated ex-vivo human crystalline lens," *Vision Res.* **49**(1), 74–83 (2009).
10. R. Urs, A. Ho, F. Manns, and J. M. Parel, "Age-dependent Fourier model of the shape of the isolated ex vivo human crystalline lens," *Vision Res.* **50**(11), 1041–1047 (2010).
11. A. M. Rosen, D. B. Denham, V. Fernandez, D. Borja, A. Ho, F. Manns, J. M. Parel, and R. C. Augusteyn, "In vitro dimensions and curvatures of human lenses," *Vision Res.* **46**(6-7), 1002–1009 (2006).
12. D. Borja, F. Manns, A. Ho, N. Ziebarth, A. M. Rosen, R. Jain, A. Amelinckx, E. Arrieta, R. C. Augusteyn, and J. M. Parel, "Optical power of the isolated human crystalline lens," *Invest. Ophthalmol. Visual Sci.* **49**(6), 2541–2548 (2008).
13. R. A. Schachar, "Central surface curvatures of postmortem- extracted intact human crystalline lenses: implications for understanding the mechanism of accommodation," *Ophthalmology* **111**, 1699–1704 (2004).
14. F. Manns, V. Fernandez, S. Zipper, S. Sandadi, M. Hamaoui, A. Ho, and J. M. Parel, "Radius of curvature and asphericity of the anterior and posterior surface of human cadaver crystalline lenses," *Exp Eye Res* **78**(1), 39–51 (2004).
15. C. E. Jones, D. A. Atchison, R. Meder, and J. M. Pope, "Refractive index distribution and optical properties of the isolated human lens measured using magnetic resonance imaging (MRI)," *Vision Res.* **45**(18), 2352–2366 (2005).
16. S. R. Uhlhorn, D. Borja, F. Manns, and J. M. Parel, "Refractive index measurement of the isolated crystalline lens using optical coherence tomography," *Vision Res.* **48**(27), 2732–2738 (2008).
17. M. Sun, J. Birkenfeld, A. de Castro, S. Ortiz, and S. Marcos, "OCT 3-D surface topography of isolated human crystalline lenses," *Biomed. Opt. Express* **5**(10), 3547–3561 (2014).
18. E. Martinez-Enriquez, A. de Castro, A. Mohamed, N. G. Sravani, M. Ruggeri, F. Manns, and S. Marcos, "Age-Related Changes to the Three-Dimensional Full Shape of the Isolated Human Crystalline Lens," *Invest. Ophthalmol. Visual Sci.* **61**(4), 11 (2020).
19. R. C. Augusteyn, A. Mohamed, D. Nankivil, P. Veerendranath, E. Arrieta, M. Taneja, F. Manns, A. Ho, and J. M. Parel, "Age-dependence of the optomechanical responses of ex vivo human lenses from India and the USA, and the force required to produce these in a lens stretcher: the similarity to in vivo disaccommodation," *Vision Res.* **51**(14), 1667–1678 (2011).
20. P. Rosales, M. Dubbelman, S. Marcos, and R. van der Heijde, "Crystalline lens radii of curvature from Purkinje and Scheimpflug imaging," *J. Vis.* **6**(10), 5 (2006).
21. L. F. Garner and M. K. Yap, "Changes in ocular dimensions and refraction with accommodation," *Opt. Phys. Opt.* **17**(1), 12–17 (1997).
22. C. A. Cook, J. F. Koretz, A. Pfahnl, J. Hyun, and P. L. Kaufman, "Aging of the human crystalline lens and anterior segment," *Vision Res.* **34**(22), 2945–2954 (1994).
23. J. F. Koretz, C. A. Cook, and P. L. Kaufman, "Aging of the human lens: changes in lens shape at zero-diopter accommodation," *J. Opt. Soc. Am. A* **18**(2), 265–272 (2001).
24. M. Dubbelman and G. L. Van der Heijde, "The shape of the aging human lens: curvature, equivalent refractive index and the lens paradox," *Vision Res.* **41**(14), 1867–1877 (2001).
25. M. Dubbelman, G. L. Van der Heijde, and H. A. Weeber, "Change in shape of the aging human crystalline lens with accommodation," *Vision Res.* **45**(1), 117–132 (2005).
26. I. Grulkowski, S. Manzanera, L. Cwiklinski, F. Sobczuk, K. Karnowski, and P. Artal, "Swept source optical coherence tomography and tunable lens technology for comprehensive imaging and biometry of the whole eye," *Optica* **5**(1), 52–59 (2018).
27. S. Ortiz, P. Perez-Merino, E. Gamba, A. de Castro, and S. Marcos, "In vivo human crystalline lens topography," *Biomed. Opt. Express* **3**(10), 2471–2488 (2012).
28. P. Pérez-Merino, M. Velasco-Ocana, E. Martinez-Enriquez, and S. Marcos, "OCT-based crystalline lens topography in accommodating eyes," *Biomed. Opt. Express* **6**(12), 5039–5054 (2015).
29. M. Sun, P. Pérez-Merino, E. Martinez-Enriquez, M. Velasco-Ocana, and S. Marcos, "Full 3-D OCT-based pseudophakic custom computer eye model," *Biomed. Opt. Express* **7**(3), 1074–1088 (2016).

30. D. A. Atchison, E. L. Markwell, S. Kasthurirangan, J. M. Pope, G. Smith, and P. G. Swann, "Age-related changes in optical and biometric characteristics of emmetropic eyes," *J. Vis.* **8**(4), 29 (2008).
31. E. A. Hermans, P. J. Pouwels, M. Dubbelman, J. P. Kuijter, R. G. van der Heijde, and R. M. Heethaar, "Constant volume of the human lens and decrease in surface area of the capsular bag during accommodation: an MRI and Scheimpflug study," *Invest. Ophthalmol. Visual Sci.* **50**(1), 281–289 (2009).
32. S. Kasthurirangan, E. L. Markwell, D. A. Atchison, and J. M. Pope, "MRI study of the changes in crystalline lens shape with accommodation and aging in humans," *J. Vis.* **11**(3), 19 (2011).
33. A. L. Sheppard, C. J. Evans, K. D. Singh, J. S. Wolffsohn, M. C. Dunne, and L. N. Davies, "Three-dimensional magnetic resonance imaging of the phakic crystalline lens during accommodation," *Invest. Ophthalmol. Visual Sci.* **52**(6), 3689–3697 (2011).
34. V. Ramasubramanian and A. Glasser, "Objective measurement of accommodative biometric changes using ultrasound biomicroscopy," *J. Cataract Refract Surg.* **41**(3), 511–526 (2015).
35. Y. S. Yoo, W. J. Whang, K. Y. Hwang, M. Lazo, J. H. Hwang, C. K. Joo, and G. Yoon, "Use of the Crystalline Lens Equatorial Plane as a New Parameter for Predicting Postoperative Intraocular Lens Position," *Am J Ophthalmol.* **198**, 17–24 (2019).
36. Y. S. Yoo, W. J. Whang, H. S. Kim, C. K. Joo, and G. Yoon, "Preoperative biometric measurements with anterior segment optical coherence tomography and prediction of postoperative intraocular lens position," *Medicine* **98**(50), e18026 (2019).
37. G. O. Waring, D. H. Chang, K. M. Rocha, L. Gouvea, and R. Penatti, "Correlation of intraoperative optical coherence tomography of crystalline lens diameter, thickness, and volume with biometry and age," *Am. J. Ophthalmol.* **225**, 147–156 (2021).
38. T. Satou, K. Shimizu, S. Tsunehiro, A. Igarashi, S. Kato, M. Koshimizu, and T. Niida, "Relationship between crystalline lens thickness and shape and the identification of anterior ocular segment parameters for predicting the intraocular lens position after cataract surgery," *BioMed Res. Int.* **2019**, 1–9 (2019).
39. E. Martínez-Enriquez, M. Sun, M. Velasco-Ocana, J. Birkenfeld, P. Perez-Merino, and S. Marcos, "Optical Coherence Tomography Based Estimates of Crystalline Lens Volume, Equatorial Diameter, and Plane Position," *Invest. Ophthalmol. Visual Sci.* **57**(9), 600–610 (2016).
40. E. Martínez-Enriquez, P. Perez-Merino, M. Velasco-Ocana, and S. Marcos, "OCT-based full crystalline lens shape change during accommodation in vivo," *Biomed. Opt. Express* **8**(2), 918–933 (2017).
41. E. Martínez-Enriquez, A. Mohamed, M. Ruggeri, M. Velasco-Ocana, S. Williams, B. Maceo Heilman, A. De Castro, P. Perez-Merino, N. Geetha Sravani, V. Sangwan, J.-M. A. Parel, R. C. Augusteyn, A. Ho, F. Manns, and S. Marcos, "Full shape crystalline lens geometrical changes with age from 3-D OCT images in vivo and ex vivo," *Invest. Ophthalmol. Visual Sci.* **59**, 268 (2018).
42. G. Muralidharan, E. Martínez-Enriquez, J. Birkenfeld, M. Velasco-Ocana, P. Pérez-Merino, and S. Marcos, "Morphological changes of human crystalline lens in myopia," *Biomed. Opt. Express* **10**(12), 6084–6095 (2019).
43. P. Pérez-Merino, M. Velasco-Ocana, E. Martínez-Enriquez, L. Revuelta, S. A. McFadden, and S. Marcos, "Three-dimensional OCT based guinea pig eye model: relating morphology and optics," *Biomed. Opt. Express* **8**(4), 2173–2184 (2017).
44. E. Martínez-Enriquez, A. de Castro, and S. Marcos, "Eigenlenses: a new model for full crystalline lens shape representation and its applications," *Biomed. Opt. Express* **11**(10), 5633–5649 (2020).
45. E. Martínez-Enriquez, A. Curatolo, A. de Castro, J. S. Birkenfeld, A. M. González, A. Mohamed, M. Ruggeri, F. Manns, Z. Fernando, and S. Marcos, "Estimation of the full shape of the crystalline lens in-vivo from OCT images using eigenlenses," *Biomed. Opt. Express* **14**(2), 608–626 (2023).
46. M. Ruggeri, S. Williams, B. M. Heilman, Y. Yao, Y. C. Chang, A. Mohamed, N. G. Sravani, H. Durkee, C. Rowaan, A. Gonzalez, A. Ho, J. M. Parel, and F. Manns, "System for on- and off-axis volumetric OCT imaging and ray tracing aberrometry of the crystalline lens," *Biomed. Opt. Express* **9**(8), 3834–3851 (2018).
47. B. Maceo Heilman, A. Mohamed, M. Ruggeri, S. Williams, A. Ho, J.-M. Parel, and F. Manns, "Age-Dependence of the Peripheral Defocus of the Isolated Human Crystalline Lens," *Invest. Ophthalmol. Visual Sci.* **62**(3), 15 (2021).
48. S. Ortiz, D. Siedlecki, P. Perez-Merino, N. Chia, A. de Castro, M. Szkulmowski, M. Wojtkowski, and S. Marcos, "Corneal topography from spectral optical coherence tomography (sOCT)," *Biomed. Opt. Express* **2**(12), 3232–3247 (2011).
49. J. M. Bland and D. G. Altman, "Statistical methods for assessing agreement between two methods of clinical measurement," *Lancet* **327**(8476), 307–310 (1986).
50. A. Khan, J. M. Pope, P. K. Verkicharla, M. Suheimat, and D. A. Atchison, "Change in human lens dimensions, lens refractive index distribution and ciliary body ring diameter with accommodation," *Biomed. Opt. Express* **9**(3), 1272–1282 (2018).
51. C. E. Jones, D. A. Atchison, and J. M. Pope, "Changes in lens dimensions and refractive index with age and accommodation," *Optom. Vis. Sci.* **84**(10), 990–995 (2007).
52. E. Martínez-Enriquez, A. De Castro, A. Mohamed, B. Maceo Heilman, S. Williams, S. Nandyala, M. Ruggeri, J.-M. A. Parel, R. Augusteyn, A. Ho, F. Manns, and S. Marcos, "3D OCT-based geometrical changes of human crystalline lenses during simulated accommodation in a lens stretcher," *Invest. Ophthalmol. Visual Sci.* **61**, 1713 (2020).
53. S. Kasthurirangan and A. Glasser, "Age related changes in accommodative dynamics in humans," *Vision Res.* **46**(8–9), 1507–1519 (2006).

54. E. Martínez-Enríquez, "Estimation of the full shape of the crystalline lens from OCT: validation using stretched donor lenses," Github, 2023, <https://github.com/EduardoMartinezEnriquez/Estimation-of-the-full-shape-of-the-crystalline-lens-from-OCT-validation-using-stretched-donor-len>.